

# Comparison of Bayesian Land Surface Temperature algorithm performance with Terra MODIS observations

John A. Morgan  
The Aerospace Corporation  
P. O. Box 92957  
Los Angeles, CA 90009

---

## Abstract

An approach to land surface temperature (LST) estimation that relies upon Bayesian inference has been tested against multiband infrared radiometric imagery from the Terra MODIS instrument. The algorithm employed requires minimal knowledge of surface emissivity, starting from a parsimoniously chosen (hence, uninformative) range of prior band emissivity knowledge. Two estimation methods have been tested. The first is the iterative contraction mapping of joint expectation values for LST and surface emissivity described in a previous paper. In the second method, the Bayesian algorithm is reformulated as a Maximum *A-Posteriori* (MAP) search for the maximum joint *a-posteriori* probability for LST, given observed sensor aperture radiances and *a-priori* probabilities for LST and emissivity.

Two MODIS data granules each for daytime and nighttime were used for the comparison. The granules were chosen to be largely cloud-free, with limited vertical relief in those portions of the granules for which the sensor zenith angle  $|ZA| < 30^\circ$ . Level 1B radiances were used to obtain 500 LST estimates per granule for comparison with the Level 2 MODIS LST product.

The Bayesian LST estimators accurately reproduce standard MODIS product LST values. In particular, the mean discrepancy for the MAP retrievals is  $|\langle \Delta T \rangle| < 0.3 K$ , and its standard deviation does not exceed  $1 K$ . The  $\pm 68\%$  confidence intervals for individual LST estimates associated with assumed uncertainty in surface emissivity are of order  $0.8 K$ .

The Appendix presents a proof of convergence of the iterative contraction mapping algorithm. The expectation values of surface temperature in multiple bands, and jointly in all bands, converge to a fixed point, within a stipulated convergence criterion. Provided the support  $[T_{min}, T_{max}]$  for the

calculation of the expectation value brackets the maximum in the joint posterior probability for LST, the fixed point converges to the MAP LST estimate in the limit  $T_{max} - T_{min} \rightarrow 0$ .

---

## 1. Introduction

Land surface temperature (LST) is a vitally important remotely observable tracer of mass and energy exchange across the interface between the atmosphere and the ground. LST derived from satellite observations is of interest in its own right for local climate studies and climate change monitoring, and as a component of studies of land cover, land cover change, surface moisture, and precision farming, among others (Dash *et al.*, 2002; Wan *et al.*, 2004). Unfortunately, few surfaces at the bottom of the atmosphere radiate as blackbodies, and the parameterization of their surface state by means of emissivities complicates the task of accurate temperature determination.

This paper continues the development of Bayesian LST estimators that do not require accurate knowledge of surface emissivity, given radiance in multiple bands (Morgan, 2005). The approach may be considered as complementary to the widespread use of regression-law based split-window algorithms.

Section 2 reviews the elements of the Bayesian LST formalism. Two implementations of the Bayesian approach have been investigated. The first is the iterative contraction mapping algorithm presented in Morgan (2005). The second is a Maximum-A Posteriori approach to LST estimation. Section 3 presents Bayesian estimates of LST and band emissivity for MODIS imagery. Section 4 discusses results, and a final Section 5 offers conclusions. Appendix A presents a proof of convergence for the iterative algorithm, and estimates of the effect on LST retrieval of uncertainty in aerosol loading.

## 2. Elements of Bayesian Land Surface Temperature Estimation

### 2.1. The Posterior Probability for $T$

We begin by recalling some of the results obtained in Morgan (2005), which may be consulted for details. The probability of sensing radiance  $I_i$  at the top of the atmosphere (TOA), given  $T$ ,  $\epsilon_i$ , and an estimate  $\sigma_i$  of the variance of the sensor radiance noise, is obtained by a Maximum Entropy (MAXENT) argument. The MAXENT estimator assumes the existence of

a forward model for the TOA radiance in terms of  $T$  and  $\epsilon_i$ . For the case of a sensor aperture radiance forward model  $I_i^{FM}$  that is *linear* in band emissivity  $\epsilon_i$ , the posterior probability  $P(I_i | T, \epsilon_i, \sigma_i)$  is Gaussian in the mismatch between  $I_i$  and  $I_i^{FM}$  in each band  $i$ . We also have

$$P(\{I_i\} | T, \{\sigma_i\}) = \prod_{i=1}^N P(I_i | T, \epsilon_i, \sigma_i). \quad (1)$$

as the posterior probability for all bands jointly.

Given radiance  $I_i$  in  $N$  bands detected at the top of the atmosphere (TOA) that originates from a patch on the Earth's surface by a sensor with noise radiance  $\sigma_i$ , the posterior probability that the surface is at a temperature  $T$  is given by Bayes' theorem as

$$P(T, \epsilon_i | I_i, K) = P(T, \epsilon_i | K) \frac{P(I_i | T, \epsilon_i, K)}{P(I_i | K)}. \quad (2)$$

Equation (2) is evaluated with aid of the prior probability for the surface to be at temperature  $T$  and emissivity  $\epsilon_i$  given available knowledge  $K$ ,

$$P(T, \epsilon_i | K) dT d\epsilon_i \propto \frac{dT}{T} d\epsilon_i, \quad (3)$$

The result is a posterior probability density. If one is ignorant of, or unconcerned with, the value of emissivity, it is possible to marginalize on the nuisance variable  $\epsilon_i$ :

$$P(T | I_i, K) = \int_{\epsilon_{min}}^{\epsilon_{max}} d\epsilon_i P(T, \epsilon_i | I_i, K) \quad (4)$$

and  $P(T | I_i, K)$ <sup>1</sup> may be expressed in closed form using error functions. The explicit form is given in Morgan (2005).

## 2.2. Land Surface Temperature Algorithms

We desire to find an estimator for surface temperature using the posterior probability given by Bayes' Theorem (2). Two LST algorithms have been developed. The first, recounted in Morgan (2005), iteratively computes

---

<sup>1</sup>In Morgan (2005), the posterior probability density was written  $P(T | I_i, K) \frac{dT}{T}$

expectation values of LST and band emissivities from their posterior probabilities while contracting the range of *a-priori* limits on these parameters.

The second calculational method is search for the maximum *A-Posteriori* probability (MAP) value of LST that maximises  $P(T | \{I_i\}, K)$ . The motivation for investigating a MAP formulation for the Bayesian LST estimator is simple. The original Bayesian LST algorithm presented in Morgan (2005) obtains estimates of LST and band emissivity by iterative refinement of expectation values for these quantities. Even though the posterior probability for surface T is a closed-form expression, this procedure is computationally intensive. Moreover, extensions to the estimator (such as, for example, a more careful treatment of the forward model, or incorporation of calibration error effects (Morgan, 2006)) may deprive us of the comfort of the closed-form solution. The MAP criterion for an estimator promises to dramatically reduce the number of CPU cycles expended per LST estimate, and may yet preserve the ability to rely upon closed-form solutions. MAP LST estimates are obtained simply and quickly by a Golden Section search.<sup>2</sup>

It was conjectured in Morgan (2005) that the iterative algorithm converges in general. Appendix A presents a proof that the iterative algorithm converges, and, in the limit, converges to the MAP estimate of LST. Granted the robustness of the Golden Section search, the existence of a solution for the MAP estimator may not appear to be a concern. However, the MAP algorithm in general includes iterative refinement of the *a-priori* limits on surface emissivity. The existence of a unique MAP estimate for LST in that case follows from a straightforward adaptation of the method of proof given in the Appendix.

### 2.3. Confidence Intervals

A desirable feature of an LST estimator is some means of assessing one's confidence in the accuracy of individual estimates. In the present case LST estimates are obtained by marginalizing over imperfectly known surface emissivities. It is naturally of great interest to explore means of judging the effect of an uninformative range for the *a-priori* probability for  $\epsilon_i$ . Direct numerical integration of the posterior probability  $P(T | \{I_i\}, K)$  with respect to  $T$  was used to calculate emissivity prior confidence intervals for LST retrievals

---

<sup>2</sup>It is not difficult to extend the MAP approach to higher dimensions by simultaneously optimizing with Powell's method on (for example) band emissivity prior limits and LST. Sample tests of such extensions show promise, but remain to be investigated systematically.

presented in this study. Suppose that LST uncertainties arising from an uninformative emissivity prior are independent of those originating from other sources of error. Then the emissivity prior confidence level may be combined with an estimate of the net effect of all other sources of error by adding in quadrature to obtain an overall LST uncertainty estimate.

### 3. Application to MODIS imagery

Both the MAP and iterative versions of the Bayesian algorithm have been applied to MODIS imagery. This effort took advantage of the availability of Level 1b calibrated radiances and Level 2 land surface temperatures (used in lieu of ground truth) for Terra MODIS data granules through the Goddard Space Flight Center (GSFC) EOS/DAAC website (Savtchenko *et al.*, 2004). Level 2 atmospheric profiles were obtained from the same site. The Level 2 surface temperature product is used in preference to the standard Level 3 product because it is in the same 1 km swath format as the Level 1 b radiance data. The GSFC-supplied HDFLook display package was used to manipulate the data granules and associated standard products.

Four MODIS data granules were selected for comparison of Bayesian LST estimates with the MOD11\_L2 LST product. To the extent possible, granules were chosen to have large areas with gentle topographic relief and minimal cloud cover effects. A list of the granules used in this study appears in Table 1. Two granules are daytime, and two nighttime. The nighttime granule for 2006 day-of-year (DOY) 258 includes the alluvial plains of Iraq and both the coastal plains and central plateau of Saudi Arabia. 2006 DOY 268, also nighttime, includes the Great Plains portion of Central Canada. 2006 DOY 350 is a daytime dataset covering Northeast Africa, including large plains in Sudan. 2006 DOY 347, also daytime, covers much of the plains of Central Asia. The MOD11\_L2 product reported LST values for approximately 75% or more of the pixels in all four granules.

Cloud-free pixels for which Level 2 MODIS LST values were reported were selected for analysis. A number of cuts were made in selecting data from the MODIS products for surface temperature estimation. The use of Level 1b radiance products combined with Level 2 atmospheric profiles to generate LST for comparison with a Level 2 MODIS temperature product introduces sources of error originating in, among others, imperfect georeferencing. Thus one may expect errors in surface altitude to affect retrieval accuracy. These effects may be exacerbated by use of bilinear interpolation

of 4 km horizontally reported profiles to the 1 km sampling of the spectral radiances. In order to minimize this source of potential error, LST retrieval was limited to sensor zenith angles  $|ZA| < 30^\circ$ . Cloudy pixels were masked by rejecting pixels for which the LST quality control mask bits 0,2,3,4, or 5 were nonzero. LST retrievals were attempted only for pixels for which the dew point temperature at the base of the water vapor profile exceeded the freezing point of water.

Cuts were also made on the basis of nonphysical or otherwise pathological fields in the granule data: Pixels for which the MODIS LST, the MODIS LST error, the surface temperature field in the profile granule (otherwise not used in the analysis), the surface air temperature at the lowest level of the profile, or the surface pressure were less than zero, were eliminated from processing. Finally, pixels for which surface pressure exceeded 1000 millibars, but for which the surface altitude was less than zero, were omitted from the analysis.

Neither ground truth nor surface meteorological range (*VSBY*) is available as a standard product with MODIS granules. However, the presence of LWIR bands in the split-window algorithm used to produce the MODIS LST product (Wan and Dozier, 1996; Wan, 1999) suggests that LST retrievals should not be too sensitive to the exact value assumed for *VSBY* in the forward model. Accordingly, this study replicates MODIS LST values assuming a nominal, but fairly large, value of  $23\text{ km}$  for the surface *VSBY* parameter for clear pixels. Appendix B presents a calculation which supports the contention that, for purposes of the present study, this approximation should not introduce large errors for clear air pixels.

A random selection of 500 pixels was made from each granule, subject to data cuts described above. LST retrievals from both single-pass MAP and two-pass iterative versions of the algorithm were obtained for all granules. In addition,  $\pm 68\%$  confidence intervals<sup>3</sup> were computed for the MAP retrievals by numerical integration of the posterior probability distribution. The bandset used in the retrievals appears in Table 2. The MODerate resolution atmospheric TRANsmission (MODTRAN4) code (Kneizys *et al.*, 1996; Berk *et al.*, 1989) was used for the forward model calculations, as described in Morgan (2005). The forward models incorporated MOD07\_L2 air tem-

---

<sup>3</sup> $\pm 68\%$  confidence levels for lack of emissivity knowledge were chosen to approximate the equivalent of  $2\sigma$  intervals, given that  $P(T | \{I_i\}, K)$  generally displays some skewness. This should be borne in mind when comparing with the effect of other error sources described by a standard deviation.

perature and water vapor profiles and assumed a  $CO_2$  mixing ratio of 382.5 ppm.

Initially, the prior probability in (3) was assumed to hold over the range

$$\begin{aligned} 200K &\leq T \leq 500K \\ 0.85 &\leq \epsilon_i \leq 0.999 \end{aligned}$$

for  $T$  and  $\epsilon$  in each band. However, it proved advantageous to restrict the range of the emissivity prior for MODIS bands 31 and 32,

$$\begin{aligned} 0.95 &\leq \epsilon_{31} \leq 0.999 \\ 0.95 &\leq \epsilon_{32} \leq 0.999 \end{aligned}$$

so as to take advantage of the observation in (Wan and Dozier 1996, Wan 1999) that most natural land cover types have an emissivity in excess of 0.97 in these bands.

In the simulated LST retrievals presented in Morgan (2005), the equivalent noise radiance  $\sigma_i$  in each band was parameterized by a signal-to-noise ratio (SNR) value obtained by approximately inverting the noise-equivalent temperature change ( $NE\Delta T$ ) for the specified nominal MODIS performance. Experimentation with actual MODIS data revealed that the SNR values so chosen greatly underestimated the random variance in radiance measured by the actual Terra spacecraft against real terrestrial surfaces, through a real, and sometimes dirty, atmosphere. In consequence, the SNR parameter was reduced from values characteristic of ideal performance, in which the only source of radiance error in sensor measurements is accounted for by  $NE\Delta T$ , by a full order of magnitude. In fact, the label "SNR" is probably somewhat misleading, since the random variability it describes is likely the concatenation of numerous confounding factors, not all of which need accurately described as "noise". It is retained because of its use in earlier studies.

The SNR values used in all retrievals reported in this study appear in Table 2. These values were selected on the basis of trial-and-error with pixels from DOY 347 that were drawn independently from the selection used for comparison with the MODIS LST product. LST estimates are fairly insensitive to the exact values chosen for band SNR's, so long as these are fairly large. If the SNR values are too large, the noise variance estimate becomes so tight that the retrieval becomes pathologically overconstrained. In the most commonly observed pathology, one or more of the individual band posterior probability fails to overlap the others; *i. e.* the support of the joint

posterior probability becomes the null set. If SNR is too small,  $\leq O(10)$  for MODIS, LST retrievals become badly biased towards underestimates, and confidence intervals become worryingly large.

Tables 3 and 4 present the mean, standard deviation and  $\chi^2$  of the mismatch for each granule for MAP and iterative retrievals, respectively. In Table 3, summary statistics for LST are shown for  $0.85 \leq \epsilon_{31,32} \leq 0.999$  as well as for  $0.95 \leq \epsilon_{31,32} \leq 0.999$ . A small number of pixels required relaxation of the SNR parameter or emissivity priors in order to obtain an iterative LST estimate, in a pattern similar to that reported in Morgan (2005).

Figures 1-8 display plots of the mismatch between MAP and MODIS LST values, with  $\pm 68\%$  confidence intervals, and of mismatch histograms, for 500 MODIS pixels from each of the four data granules. Overplotted on each mismatch histogram is the histogram for the equivalent Gaussian error distribution

$$P(\delta T) = \frac{1}{\sqrt{2\pi}\sigma} \exp\left(-\frac{(\delta T - \langle \delta T \rangle)^2}{2\sigma^2}\right). \quad (5)$$

Note that the confidence intervals in the plots (whose mean and standard deviation for each granule is given in the LST mismatch figure captions) are for the uncertainty in LST resulting from the assumed uncertainty prior for surface emissivity only. Thus, they do not (directly) reflect sensor noise effects or other sources of uncontrollable variance.<sup>4</sup>

#### 4. Discussion

Agreement between the Level 2 MODIS LST product and MAP LST estimates obtained in this study is better than 1  $K$  in both mean and standard deviation of the mismatch for all granules. On average, the mismatch with MODIS LST in Table 3 increases only slightly for the looser emissivity prior. In addition to the tendency for the Bayes LST retrievals to display a slight negative bias with respect to the MODIS product (consistent with the observation made in Morgan (2005)) the mismatch plots show evidence of a positive trend in the discrepancy with respect to MODIS LST. The trend is

---

<sup>4</sup>These other sources of variance do enter the confidence interval through the MAXENT estimator for the mismatch between sensor and forward model radiance. Thus, the width of the confidence interval for emissivity uncertainty depends upon what value for the SNR parameter is used in the retrieval.

readily apparent to the eye for the daytime retrievals, but can also be discerned in Figure 3 for (nighttime) DOY 268. MAP and iterative solutions reproduce MODIS LST comparably well. Only the DOY 347 retrieval shows a notably different mean mismatch compared to MODIS between iterative and MAP approaches. For both algorithms,  $\chi^2$  per degree of freedom (*DOF*) is close to unity.

The best estimate of MODIS LST accuracy lies in the range  $\pm 0.6 K$  to  $\pm 1.0 K$  (Wan *et al.*, 2004; Guenther *et al.*, 2002). The standard deviation of the MAP temperature mismatch in Table 3 also lies in this range. A t-test shows the difference in means between MODIS and MAP LST values to be statistically significant for both nighttime granules and marginally (at the 5% level) for DOY 347. However, the generally small level of the discrepancy indicates that, given better control of error sources, the Bayesian MAP algorithm is capable of replicating the accuracy of the MODIS MOD11\_L2 product.

A small number of retrievals for both algorithms have large discrepancies with respect to MOD11\_L2 LST. The cosmetic effect of these retrievals in the mismatch plots may give an exaggerated impression of their effect on the accord between MODIS and Bayesian LST. Judging from the mismatch histograms, they appear to be outliers resulting from pixels whose radiometric accuracy has been compromised by one or more of the error sources described earlier, despite imposition of the data cuts. In the case of the granule for DOY 2006/350, two pixels out of 500 have a discrepancy in excess of  $4 K$ . These discrepant values appear significantly out-of-family with respect to the largely Gaussian appearance and favorable  $\chi^2$  statistic for the retrievals as a whole. In Table 3, the summary statistics for DOY 350 are replicated with the two worst outlier pixels removed in the rows marked with an asterisk, with minimal change to the results.

Error sources arising from georeferencing errors in Level 1b radiance products have already been discussed. An additional possible origin for the discrepancies with MODIS LST is errors in the forward model. Among other causes, these could result from the fixed choice of  $V_{SBY} = 23 km$  (*vide.* Appendix B, however), or occur as a consequence of using erroneous values of air temperature or water vapor from the MOD07\_L2 profiles in MODTRAN (Wan *et al.* 2004). Another possible source is imperfect cloud masking in the Level 2 MODIS products that could corrupt pixel radiances. This last source of error would afflict MODIS LST as well, and would have to affect MODIS and Bayesian LST differentially in order to contribute to discrepancies. Fi-

nally, the assumed band emissivity prior range need not always bracket the actual surface emissivity for a pixel.

A noteworthy feature of the LST retrievals reported for this study is the comparatively small uncertainty for *individual* LST estimates originating in the assumed lack of surface emissivity knowledge. The mean value of the  $\pm 68\%$  interval for individual granules is greatest for DOY 350 (daytime) at  $0.828 \pm 0.055 K$  and least for DOY 268 (nighttime) at  $0.638 \pm 0.014 K$ . As noted earlier, the emissivity uncertainty confidence interval depends upon the assumed level of random variance due to noise and other uncontrollable factors capable of influencing LST retrieval. However, insensitivity of Bayesian LST to emissivity seems likely to hold generally. In particular, confidence intervals for  $\epsilon_{31,32} \geq 0.85$  differ little from those for  $\epsilon_{31,32} \geq 0.95$

It was remarked earlier that the Bayesian approach to LST estimation was complementary to the more common split-window algorithmic family. The MODIS generalized split-window algorithm that furnished LST values against which performance of the Bayes approach has been tested relies upon regression against a large training dataset, and requires assignment of pixels to emissivity classes. The Bayesian approach, while statistical in its treatment of emissivity uncertainty, relies upon radiative transfer theory, rather than regression of brightness temperatures against true LST, to invert radiance to surface temperature. It is thus a method of remotely determining LST that (so to speak) minimizes hostages to the fortunes of emissivity knowledge. The accurate reproduction in the mean of MOD11\_L2 LST in this study suggests the possibility of using the Bayesian approach for virtual "ground truth" to train local or regional split-window LST algorithms.

Although the golden section search for the MAP version runs faster than the iterative solution in prototype IDL (Interactive Data Language) code, the difference in execution time is not great, and is in any event dominated by the execution time for the forward model calculations in MODTRAN. However, the MAP version of the algorithm would seem preferable both on the basis of simplicity and because it readily admits extension to higher-dimensional searches for optimal joint estimates of LST and band emissivity.

## 5. Conclusion

The performance of the Bayesian land surface temperature retrieval algorithms has been tested in a small-scale study by comparison of Bayesian

LST estimates against the MODIS MOD11\_L2 LST product. Both the original iterative contraction mapping search and a new Maximum *A-Posteriori* algorithm reproduce MODIS LST values with good accuracy. The mean mismatch with respect to the MOD11\_L2 LST product for Maximum *A-Posteriori* estimates does not exceed  $0.3 K$ , and its standard deviation is less than  $1 K$ , for any granule used in this study. For the iterative algorithm, the corresponding mean mismatch does not exceed  $0.5 K$ , nor its standard deviation,  $1.4 K$ .

The agreement of the MAP estimates derived from MODIS Level 1B radiance with the MOD11\_L2 LST is comparable to the claimed accuracy for MODIS LST. Emissivity prior confidence intervals for individual LST estimates shown in Section 4 show that LST retrieval accuracy with the Bayesian approach is insensitive to modest uncertainties in surface emissivity. We conclude the MAP LST algorithm is a viable candidate for LST retrieval in circumstances in which band emissivities are poorly known.

It has been shown (*vide*. Appendix A) that the iterative refinement of expectation values underlying the TES algorithm presented in Morgan (2005) converges, in general. In the limit of vanishing support for the LST expectation values, the iterative approach is equivalent to the Maximum *A-Posteriori* estimator for LST.

*Acknowledgement:*

I wish to thank an anonymous referee for Morgan (2005) for suggesting the Maximum-*A-Posteriori* approach.

## Appendix A. Convergence of iterative LST retrieval

The algorithm used in Morgan (2005) iteratively refines the calculation of the expectation values (A.1)-(A.3) below of surface temperature and emissivity in multiple bands by systematic contraction of the limits of integration. It has been found that this procedure, which is described in detail in (Morgan 2005), converges rapidly and reliably in practice. However, to date there has been no proof that the algorithm actually converges in general. This Appendix supplies such a proof.

For reference, the expectation values for  $T$  given radiance in bands  $i$ , obtained from the joint posterior probability for observing radiances  $I_i, i = 1, N$  are

$$\langle T_i \rangle = \frac{\int_{T_{min}}^{T_{max}} TP(T | I_i, \sigma_i)}{\int_{T_{min}}^{T_{max}} P(T | I_i, \sigma_i)}, \quad (\text{A.1})$$

assuming  $T$  is known to lie between a minimum and a maximum, while a joint estimator for  $\mathbf{T}$  given radiances in all  $N$  bands is

$$\langle T_J \rangle = \frac{\int_{T_{min}}^{T_{max}} TP(T | \{I_i\}, \{\sigma_i\})}{\int_{T_{min}}^{T_{max}} P(T | \{I_i\}, \{\sigma_i\})} \quad (\text{A.2})$$

An estimator for the emissivity in band  $i$  is given by

$$\langle \epsilon_i \rangle = \frac{\int_{\epsilon_{min}}^{\epsilon_{max}} \epsilon P(\langle T_i \rangle, \epsilon | I_i, \sigma_i) d\epsilon}{\int_{\epsilon_{min}}^{\epsilon_{max}} P(\langle T_i \rangle, \epsilon | I_i, \sigma_i) d\epsilon} \quad (\text{A.3})$$

#### *Appendix A.1. Assumptions*

Both surface temperature and band emissivities are assumed to lie within limits imposed *a-priori*. The surface temperature is limited to the range

$$T_{min} \leq T \leq T_{max}. \quad (\text{A.4})$$

and emissivity to the range

$$\epsilon_{min} \leq \epsilon_i \leq \epsilon_{max} \quad (\text{A.5})$$

where the minimum and maximum values may be band-dependent.

It is assumed that the maximum of  $P(T | \{I_i\}, K)$  is always included in the integration. In any workable procedure for iteratively refining surface temperature or emissivity by contracting the support  $[T_{min}, T_{max}]$  of the integrations (A.1-A.3) which define  $\langle \mathbf{T} \rangle$  and  $\langle \epsilon_i \rangle$ , that support must bracket the maximum of  $P(T | \{I_i\}, K)$  as it contracts. Otherwise, the most probable values of  $\langle \mathbf{T} \rangle$  and  $\langle \epsilon_i \rangle$  would be excluded from the search, in violation of the MAXENT assumption that expected values should maximize the likelihood.

#### *Appendix A.2. Proof of Convergence*

*Proposition:* The iterative refinement of (A.1)-(A.2) converges.

For clarity we limit the discussion to (A.1) and (A.2). The extension to accomodate (A.3) is clear. A total of  $N + 1$  expectation values for surface temperature  $\langle T_i \rangle$  (the index  $i$  now including the joint estimate) is obtained at each stage of iteration. The values  $\langle T_i \rangle$  comprise a vector in  $\mathbf{R}^{N+1}$ . These are confined within the subset of  $\mathbf{R}^{N+1}$  delimited by (A.4) that provides nonvanishing support for the integrations in the definitions (A.1) and (A.2). Call the vector of expectation values  $\langle \mathbf{T} \rangle$ .

At the  $n$ -th stage of iteration,  $\langle \mathbf{T} \rangle$  is calculated over the range  $[T_{min}^n, T_{max}^n]$  and the mismatch amongst the band LST expectation values  $\langle T_i \rangle$  is scored by

$$\Delta(\langle \mathbf{T} \rangle) \equiv \max |\langle T_i \rangle - \langle T_j \rangle| \quad (\text{A.6})$$

taken over all pairs of estimates. Let the set  $\mathbf{X} = \{\mathbf{x}\}$  be the set of all  $m$ -tuplets of the form

$$\mathbf{x} \equiv \left( \begin{array}{c} T_{max}^n - T_{min}^n \\ \{|\langle T_i \rangle - \langle T_j \rangle|, \forall i, j \leq N + 1\} \end{array} \right) \quad (\text{A.7})$$

consistent with the overall limits (A.4). Here

$$m \equiv \binom{N + 1}{2} + 1, \quad (\text{A.8})$$

where the quantity in parentheses is the binomial coefficient. The set  $\mathbf{X}$  is compact, so all components of any sequence  $\in \mathbf{X}$  are bounded. (They are all nonnegative, as well.) Given points  $\mathbf{x}^1, \mathbf{x}^2 \in \mathbf{X}$  define a metric function

$$d(\mathbf{x}^1, \mathbf{x}^2) \equiv \sum_{i=1, N} |x_i^1 - x_i^2|. \quad (\text{A.9})$$

The pair  $(\mathbf{X}, d)$  can be shown to be a complete metric space (Aliprantis and Burkinshaw, 1981, p. 35).

Define the function  $\zeta : \mathbf{X} \rightarrow \mathbf{R}$  by

$$\zeta(\mathbf{x}) \equiv \theta \sum_{i=1, N} x_i \geq 0. \quad (\text{A.10})$$

where  $\theta > 1$ .

Consider a contractive sequence  $x_i^n$  in  $\mathbf{X}$  with  $n = 1, 2, \dots$  for which

$$x_i^n \geq x_i^{n+1}, \forall n \quad (\text{A.11})$$

Define the mapping from one iterate of  $\mathbf{x}$  to another in  $\mathbf{X}$  by

$$\mathbf{x}^{n+1} \equiv M(\mathbf{x}^n). \quad (\text{A.12})$$

The function  $\zeta : \mathbf{X} \rightarrow \mathbf{R}$  is lower semicontinuous, and  $M : \mathbf{X} \rightarrow \mathbf{X}$  is continuous, on  $\mathbf{X}$ . By Caristi's fixed-point theorem (Ok, 2007) the mapping

$M$  has a fixed point  $M(\mathbf{x}) = \mathbf{x}$ . The iterative refinement of  $\langle \mathbf{T} \rangle$  therefore converges in  $\mathbf{X}$ . Moreover, if

$$\begin{aligned} \lim_{n \rightarrow \infty} T_{min}^n &\equiv T_{min}^\infty \\ \lim_{n \rightarrow \infty} T_{max}^n &\equiv T_{max}^\infty, \end{aligned} \quad (\text{A.13})$$

then

$$T_{min}^\infty \leq \langle T_i \rangle \leq T_{max}^\infty \quad (\text{A.14})$$

by the definition of  $\langle \mathbf{T} \rangle$ .  $\square$

### *Appendix A.3. Iterative algorithm and maximum a-Posteriori probability search*

The fixed point of the iterative mapping drives  $\Delta \rightarrow \Delta^\infty$ , returning an  $N + 1$ -tuple of LST expectation values, none of which differ from any of the others by an amount greater than  $\Delta^\infty$ . It may appear that nothing in the result just obtained says any such estimate necessarily gives an accurate value for LST. In practice, however, it happens that a small number of iterations suffices to yield accurate LST estimates.

The manner in which  $T_{max} - T_{min}$  contracts remains at our disposal. We are at liberty to force it to tend to zero. We now show that  $T_{max} - T_{min} \rightarrow 0$  is equivalent to a contractive mapping chosen with

$$x_i^n > x_i^{n+1}, \forall n \quad (\text{A.15})$$

rather than (A.11), and that as  $n \rightarrow \infty$   $\langle T_i \rangle$  converges to the Maximum *A-Posteriori* estimate  $T_{MAP}$ .

The support for the computation of  $\langle \mathbf{T} \rangle$  tends to zero as  $x \rightarrow 0$ . There is thus a nested sequence of intervals  $[T_{min}^{n+1}, T_{max}^{n+1}] \subset [T_{min}^n, T_{max}^n]$ . Cantor's theorem on the intersection of a nested sequence (Aliprantis and Burkinshaw, 1981, p. 32) implies the limit of this process will be a singleton in  $\mathbf{X}$ . It was assumed at the outset that the support of integrations  $[T_{min}^n, T_{max}^n]$  in (A.1-A.2) brackets  $T_{MAP}$ ; the singleton thus corresponds to  $T = T_{MAP}$ , which is also the value of  $\langle T_J \rangle$ . We may see this last by the following argument: In

$$\langle T_J \rangle = \frac{\int_{T_{min}}^{T_{max}} TP(T | \{I_i\}, \{\sigma_i\})}{\int_{T_{min}}^{T_{max}} P(T | \{I_i\}, \{\sigma_i\})} \quad (\text{A.16})$$

as  $T_{min}, T_{max} \rightarrow T_{MAP}$ , we may write

$$\langle T_J \rangle = \int_{-\infty}^{\infty} dT f(T)T \quad (\text{A.17})$$

with

$$f(T) = \begin{cases} \frac{P(T|\{I_i\},\{\sigma_i\})}{\int_{T_{min}}^{T_{max}} P(T|\{I_i\},\{\sigma_i\})}, & T_{min} \leq T \leq T_{max} \\ \text{else } 0 \end{cases} \quad (\text{A.18})$$

As  $T_{max} - T_{min} \rightarrow 0$ , it can be shown (Lighthill, 1960) that

$$f(T) \rightarrow \delta(T - T_{MAP}) \quad (\text{A.19})$$

and thus

$$\langle T_J \rangle \rightarrow T_{MAP}. \quad (\text{A.20})$$

As  $x \rightarrow 0$ ,  $\Delta \rightarrow 0$  and the other expectation values  $\langle T_i \rangle \rightarrow T_{MAP}$ , a unique converged surface temperature estimate. Conversely, if  $T_{max}^n - T_{min}^n \rightarrow 0$ ,  $\langle \mathbf{T} \rangle \rightarrow \mathbf{T}_{MAP}$  by applying the preceding argument to each expectation value separately, and  $x \rightarrow 0$ . Then a subsequence  $x^n$  exists that respects (A.15). We thus have the

*Corollary:* In the limit  $T_{max}^n - T_{min}^n \rightarrow 0$ , iterative refinement of unbiased expectation values, *i.e.*, those for which  $\text{supp}\langle \mathbf{T} \rangle$  brackets the maximum of the  $P(T | \{I_i\}, K)$ , is equivalent to the Maximum *A-Posteriori* (MAP) approach, in which one searches directly for the value of  $T$  which maximizes the joint posterior probability (1).  $\square$

This result is likewise true of the straightforward extension of the proof given here to the case of a contractive iterative search for a fixed point for  $\langle T, \epsilon_i \rangle$ .

## Appendix B. Insensitivity of LST estimates to meteorological range

The contribution of aerosol loading of the atmosphere to the forward model radiance calculations was parameterized by specifying the surface meteorological range, or visibility (*VSBY*). This is the variable used by MODTRAN to scale aerosol extinction. The meteorological range was assumed to be 23 km for all retrievals presented in the main body. Because LST retrievals were only attempted for cloud-free pixels in what were judged to be reasonably clear air conditions, it seems reasonable to suppose that this assumption should not introduce significant error so long as few pixels have  $VSBY < 23 \text{ km}$ . We now examine the likely validity of this assumption.

We begin by adapting the analysis of Morgan (2005, 2006) to obtain the prior probability for surface meteorological range *VSBY* and use it to construct posterior probabilities marginalized over a range of *VSBY*. The

starting point is the apparently trivial observation that the meteorological range is a *length*: Traditionally, and loosely, *VSBY* is the distance at which an observer looking horizontally at a height of two meters just fails to discern the contrast presented by an object against the horizon. In the remote sensing of objects by electromagnetic radiation, Poincaré invariance requires that any two observers must be able to relate their description of events by a Lorentz transformation. In particular, the relation between  $VSBY = V$  as observed at time  $t$  in primed and unprimed coordinate systems moving with relative velocity  $v = \beta c$  with respect to each other along a stipulated line of sight (which might as well be taken to be parallel to the ground plane) is given by

$$V = \gamma(V' - \beta t') \tag{B.1}$$

$$t = \gamma(t' - \beta V') \tag{B.2}$$

where

$$\gamma = \frac{1}{\sqrt{1 - \beta^2}}. \tag{B.3}$$

The two observers will assign prior probabilities for the occurrence of particular values of the meteorological range

$$f(V)dV \tag{B.4}$$

in the unprimed system and

$$g(V')dV' \tag{B.5}$$

in the primed one. In order for observers to agree as to the form of the estimator, the priors must be related by

$$g(V')dV' = J^{-1}f(V)dV \tag{B.6}$$

where

$$J = \frac{\partial V}{\partial V'} = \gamma \tag{B.7}$$

is the Jacobian for the transformation between descriptions in the parameter space. Primed and unprimed observers, if equally cogent, must also agree as to the functional form of the prior probability for  $V$ , thus

$$f(V) = g(V) \tag{B.8}$$

leading to a form of Schröder’s equation for  $f$ ,

$$f(V) = \gamma f(\gamma V), \quad (\text{B.9})$$

with solution

$$f(V) = \frac{\text{const.}}{V} \quad (\text{B.10})$$

for the prior probability. We conclude that the  $VSBY$  parameter, with dimensions of a length, is a scale parameter, for which the prior probability takes the Jeffreys form (B.10) (Jaynes, 1968).

The prior probability (B.10) may be inserted into an estimator for LST which marginalizes on both surface emissivity and  $VSBY$  in each band  $i$ ,

$$P(T | I_i, \sigma_i) = \int_{VSBY_<}^{VSBY_>} \int_{\epsilon_{min}}^{\epsilon_{max}} P(T | I_i, \epsilon, V, \sigma_i) d\epsilon \frac{dV}{V}, \quad (\text{B.11})$$

from which a joint posterior probability may be calculated as a function of LST. This quantity may be used to compute MAP estimates of LST and confidence intervals. The estimator will now be used to examine the sensitivity of LST estimates when  $VSBY$  was allowed to vary over a range of values by means of an illustrative sample calculation.

LST MAP retrievals and confidence intervals as a function of  $VSBY_<$  for one of the pixels used in the DOY 350 granule comparison with MODIS LST appear in Figure 9.<sup>5</sup> The  $\pm 68\%$  confidence intervals shown account for the effects of the  $VSBY$  and emissivity priors only, and include no estimate of uncertainty originating from noise effects. The upper limit on the visibility prior was fixed at  $VSBY_> = 50 \text{ km}$ . The surface T prior for these retrievals was constrained to the range  $306 \text{ K} \leq T \leq 317 \text{ K}$ .

The values of LST and associated confidence intervals for this example cannot be directly compared with the MAP value 311.79 K marginalized on surface emissivity alone. However, note that the range of LST variation in Figure 9 is limited, even within the constrained LST prior limits. Moreover, the confidence intervals tend to a fixed range (consistent with the MODIS LST value) as  $VSBY$  increases. These observations provide a degree of empirical support for the assumption that the LST retrievals presented in the main text should not be too sensitive to the exact value of  $VSBY$  used

---

<sup>5</sup>A calculation for a single pixel is given because the use of nested Romberg quadratures, in which the innermost loop invokes MODTRAN, is computationally intensive.

to parameterize aerosol loading in the forward model, so long as the actual *VSBY* is great enough.

## References

## References

- ALIPRANTIS, C. S., AND O. BURKINSHAW, 1981, *Principles of Real Analysis*, (New York:North Holland)
- BERK, A., G. P. ANDERSEN, P. K. ACHARYA, J. H. CHETWYND, L. S. BERNSTEIN, E. P. SHETTLE, M. W. MATTHEW, AND S. M. ADLER-GOLDEN, 1999, *MODTRAN<sub>4</sub> User's Manual*, Air Force Research Laboratory, Hanscom AFB, MA
- DASH, P., F.-M. GÖTTSCHE, F.-S. OLESEN, AND H. FISCHER, 2002, Land surface temperature and emissivity estimation from passive sensor data: theory and practice-current trends, *Int. J. Remote Sensing*, 23, pp. 2563-2594
- GUENTHER, B., X. XIONG, V. V. SALMONSON, W. L. BARNES, AND J. YOUNG 2002, On-orbit performance of the Earth Observing System Moderate Resolution Spectroradiometer; first year of data, *Rem. Sens. Env.* 83, pp. 16-30
- JAYNES, E, 1968, Prior Probabilities, *IEEE Trans. on Systems Science and Cybernetics*, SSC-4, pp. 227-241
- KNIEZYS F., D. C. ROBERTSON, L W ABREU, P. ACHARYA, G. P. ANDERSON, L. S. ROTHMAN, J. H. CHETWYND, J. E. A. SELBY, E. PL SHETTLE, W. O. BALLERY, A. BERK, S. A. CLOUGH, AND L. S. BERNSTEIN, 1996, *The MODTRAN 2/3 Report and LOWTRAN 7 Model*, Phillips Laboratory, Hanscom AFB, MA
- LIGHTHILL, M. J, 1960, *Fourier Analysis and Generalized Functions*, (London: Cambridge University Press)
- MORGAN, J. A, 2005, Bayesian Estimation for Land Surface Temperature Retrieval: The Nuisance of Emissivities, *IEEE Trans. Geosci. Remote Sensing*, 43, pp. 1279-1288

- MORGAN, J. A., 2006, A Bayesian Estimator for Linear Calibration Error Effects in Thermal Remote Sensing, *IEEE Geosci. and Remote Sensing Letters*, 3 (1), p. 117
- OK, E. A., 2007, *Real Analysis with Economic Applications*, Princeton University Press, Princeton, p. 238
- SAVTSCHENKO, A., D. OUZOUNOV, S. AHMAD, J. ACKER, G. LEPTOUKH, J. KOSIANA, AND D. NICKLESS, 2004, Terra and Aqua MODIS products available from NASA GES DAAC, *Advances in Space Research*, 34, pp. 710-714
- WAN, Z.-M., 1999 *MODIS Land-Surface Temperature Algorithm Theoretical Basis Document*, Institute for Computational Earth System Science, University of California, Santa Barbara
- WAN, Z., AND J. DOZIER, 1996, A Generalized split-window algorithm for retrieving land-surface temperature from space, *IEEE Trans. Geosci. Remote Sens.*, 34, no. 4, pp. 892-905
- WAN, Z., Y. ZHANG, Q. ZHANG, AND Z.-L. LI, 2004, Quality assessment and validation of the MODIS global land surface temperature, *Int. J. Remote Sensing*, 25, pp. 261-274

Table 1. MODIS granule datasets

---

MOD021KM.A2006258.1900.005.2006260185940.hdf  
 MOD021KM.A2006268.0455.005.2006270054543.hdf  
 MOD021KM.A2006347.0615.005.2006348125833.hdf  
 MOD021KM.A2006350.0830.005.2006352011824.hdf  
 .....  
 MOD11\_L2.A2006258.1900.004.2006259185248.hdf  
 MOD11\_L2.A2006268.0455.004.2006269162220.hdf  
 MOD11\_L2.A2006347.0615.004.2006349135340.hdf  
 MOD11\_L2.A2006350.0830.004.2006351140447.hdf  
 .....  
 MOD07\_L2.A2006258.1900.005.2006260192510.hdf  
 MOD07\_L2.A2006268.0455.005.2006270062431.hdf  
 MOD07\_L2.A2006347.0615.005.2006348132045.hdf  
 MOD07\_L2.A2006350.0830.005.2006352015143.hdf

Table 2. MODIS band definitions, SNR parameters

MODIS band	wavelength limits	SNR
20	3.660-3.840 $\mu m$	25
22	3.929-3.989 $\mu m$	25
23	4.020-4.080 $\mu m$	25
29	8.400-8.700 $\mu m$	25
31	10.870-11.280 $\mu m$	50
32	11.770-12.270 $\mu m$	50

Table 3. Maximum *A-Posteriori* surface temperature results: mean mismatch, standard deviation, maximum mismatch, and  $\chi^2$  per degree of freedom (DOF). Results are given for two choices for the lower limit to the emissivity prior in bands 31 and 32. The rows labeled with an asterisk differs from those immediately above it by omission of the pixels with the worst two mismatches compared to MODIS LST

Granule	$\langle LST \text{ mismatch} \rangle$	$ Max \text{ mismatch} $	$\chi^2/DOF$
$0.95 \leq \epsilon_{31,32} \leq 0.999$ :			
258.1900	$0.238 \pm 0.723 K$	3.121 <i>K</i>	1.106
268.0455	$-0.286 \pm 0.416$	3.039	1.470
347.0615	$-0.058 \pm 0.672$	2.790	1.005
350.0830	$-0.036 \pm 1.043$	6.974	0.999
350.0830*	$-0.059 \pm 0.975$	3.462	1.002
.....			
$0.85 \leq \epsilon_{31,32} \leq 0.999$ :			
258.1900	$0.454 \pm 0.738 K$	3.082 <i>K</i>	1.376
268.0455	$-0.209 \pm 0.429$	2.980	1.236
347.0615	$0.100 \pm 0.731$	3.249	1.017
350.0830	$0.216 \pm 1.109$	8.866	1.036
350.0830*	$0.189 \pm 1.019$	3.737	1.032

Table 4. Iterative surface temperature results: mean mismatch, standard deviation, maximum mismatch, and  $\chi^2/DOF$

Granule	$\langle LST \text{ mismatch} \rangle$	$ Max \text{ mismatch} $	$\chi^2/DOF$
258.1900	$0.263 \pm 0.690 K$	2.856 <i>K</i>	1.143
268.0455	$-0.295 \pm 0.425$	3.220	1.480
347.0615	$-0.670 \pm 0.966$	4.081	1.480
350.0830	$0.038 \pm 1.355$	7.789	0.999

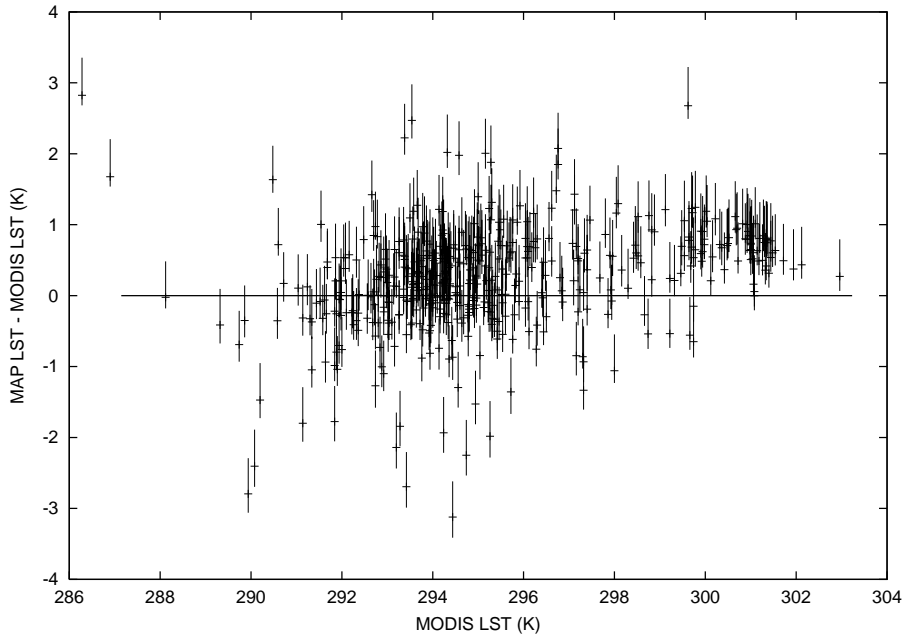


Figure .1: Mismatch between MAP and MODIS LST for 500 nighttime pixels from DOY 2006/258 granule. Mean confidence interval  $\langle \Delta T \rangle = 0.730 \pm 0.028 K$ . Confidence intervals reflect effects of emissivity uncertainty only.

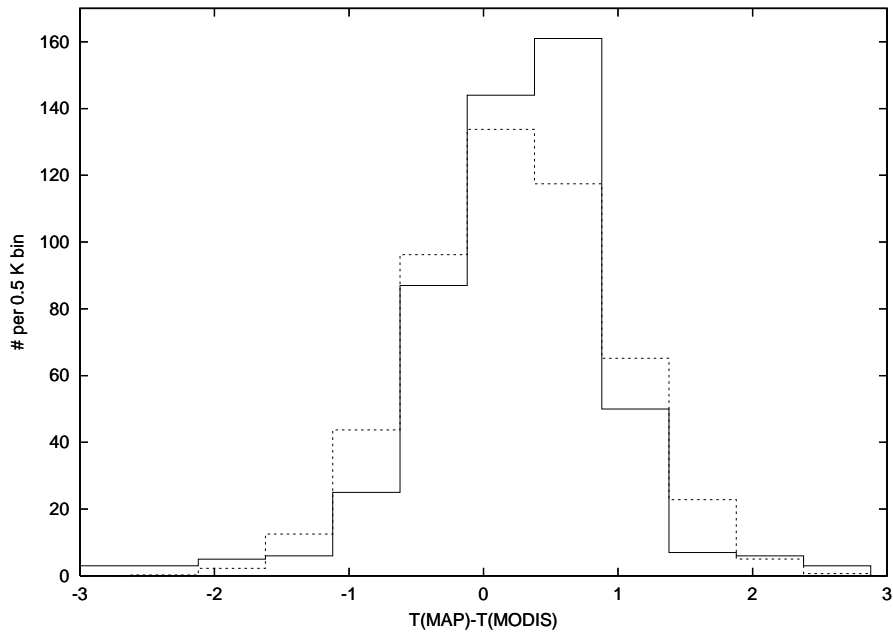


Figure .2: Nighttime MAP vs. MODIS LST mismatch histogram for DOY 2006/258. Solid line: MAP-MODIS mismatch; dashed line: Equivalent Gaussian histogram corresponding to  $\langle \delta T \rangle = 0.238 K$ ,  $\sigma = 0.723 K$ . 22

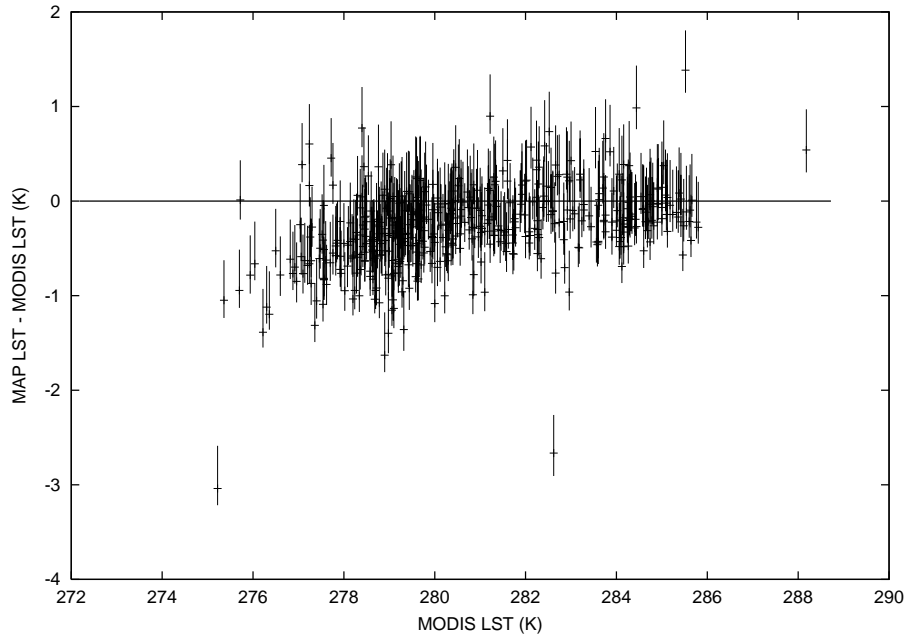


Figure .3: Mismatch between MAP and MODIS LST for 500 nighttime pixels from DOY 2006/268 granule. Mean confidence interval  $\langle \Delta T \rangle = 0.638 \pm 0.014 K$

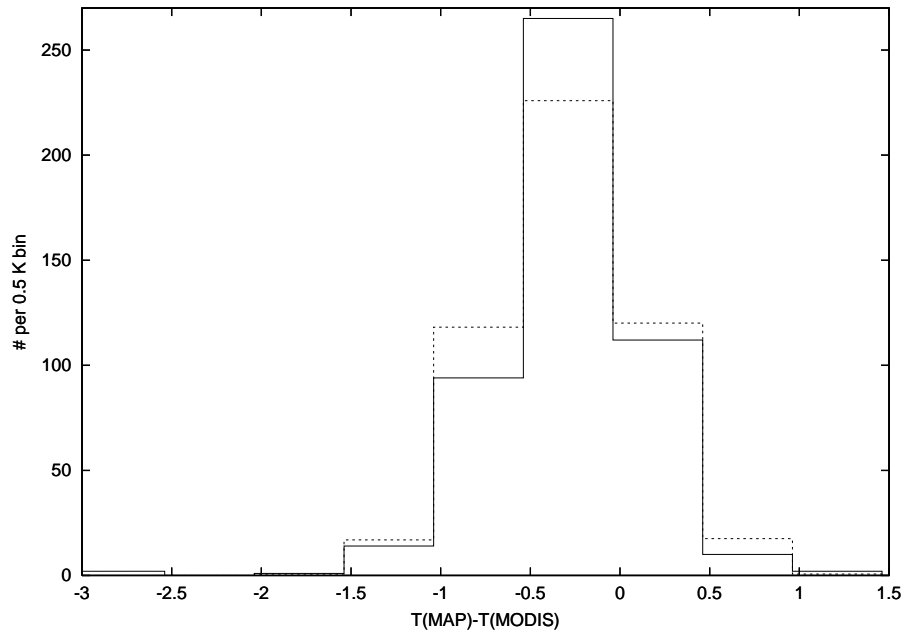


Figure .4: Nighttime MAP vs. MODIS LST mismatch histogram for DOY 2006/268. Equivalent Gaussian histogram:  $\langle \delta T \rangle = -0.286 K$ ,  $\sigma = 0.416 K$ .

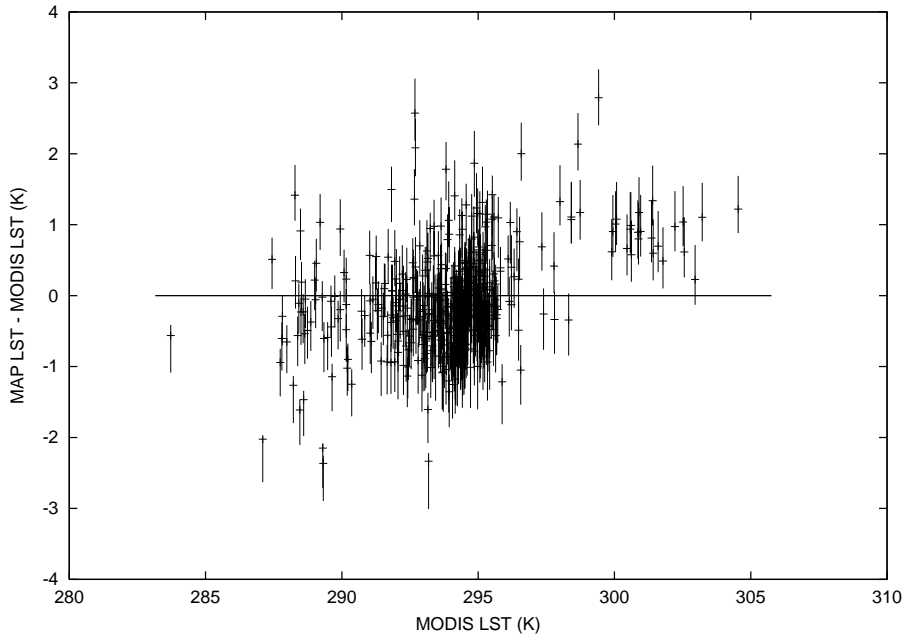


Figure .5: Mismatch between MAP and MODIS LST for 500 daytime pixels from DOY 2006/347 granule. Mean confidence interval  $\langle \Delta T \rangle = 0.796 \pm 0.054 K$

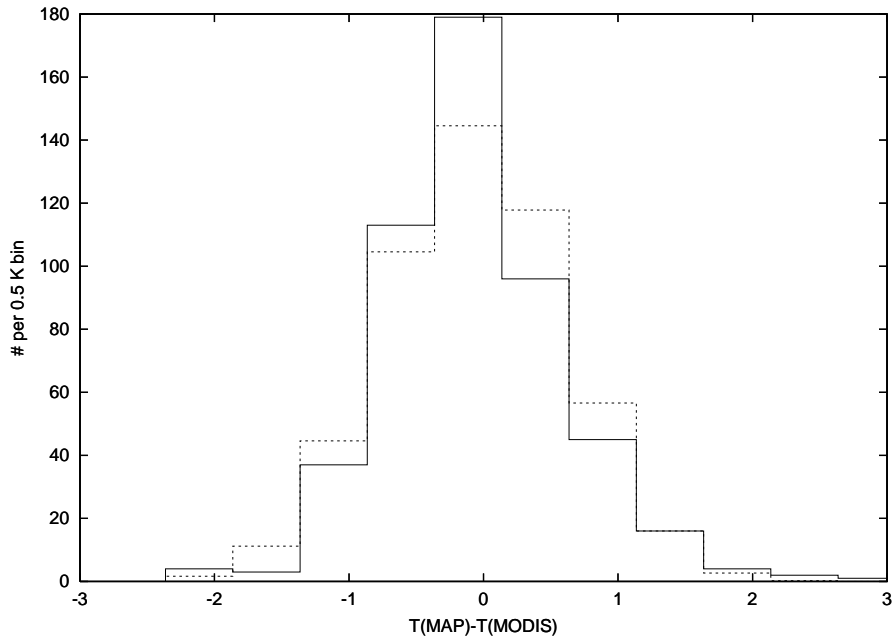


Figure .6: Daytime MAP vs. MODIS LST mismatch histogram for DOY 2006/347. Equivalent Gaussian histogram:  $\langle \delta T \rangle = -0.058K, \sigma = 0.672K$ .

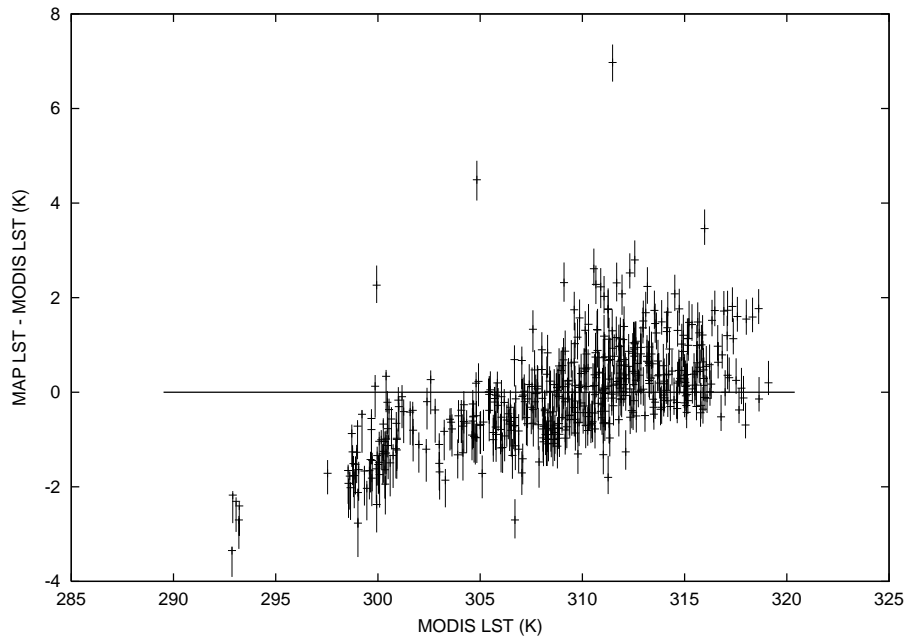


Figure .7: Mismatch between MAP and MODIS LST for 500 daytime pixels from DOY 2006/350 granule. Mean confidence interval  $\langle \Delta T \rangle = 0.828 \pm 0.055 K$

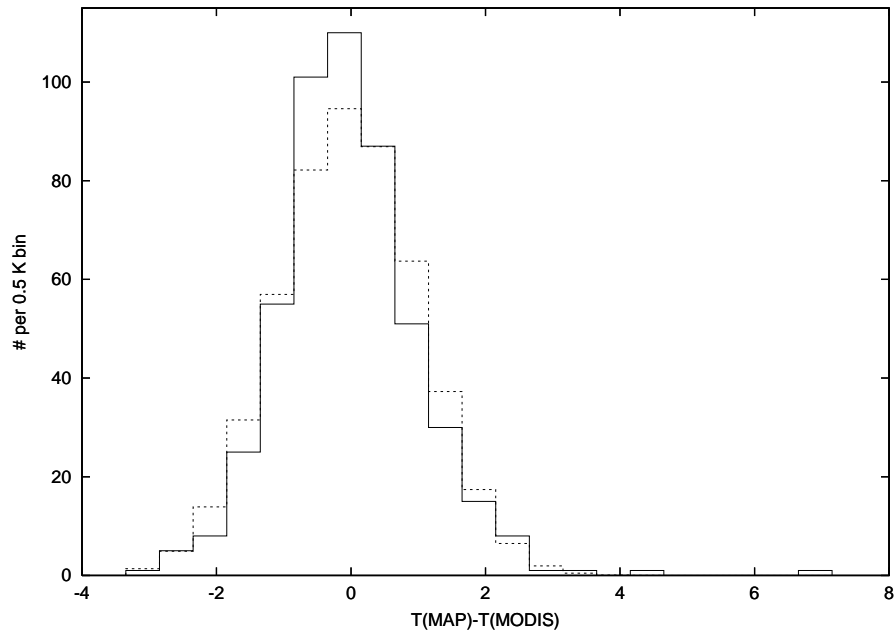


Figure .8: Daytime MAP vs. MODIS LST mismatch histogram for DOY 2006/350. Equivalent Gaussian histogram:  $\langle \delta T \rangle = -0.036 K$ ,  $\sigma = 1.043 K$ .

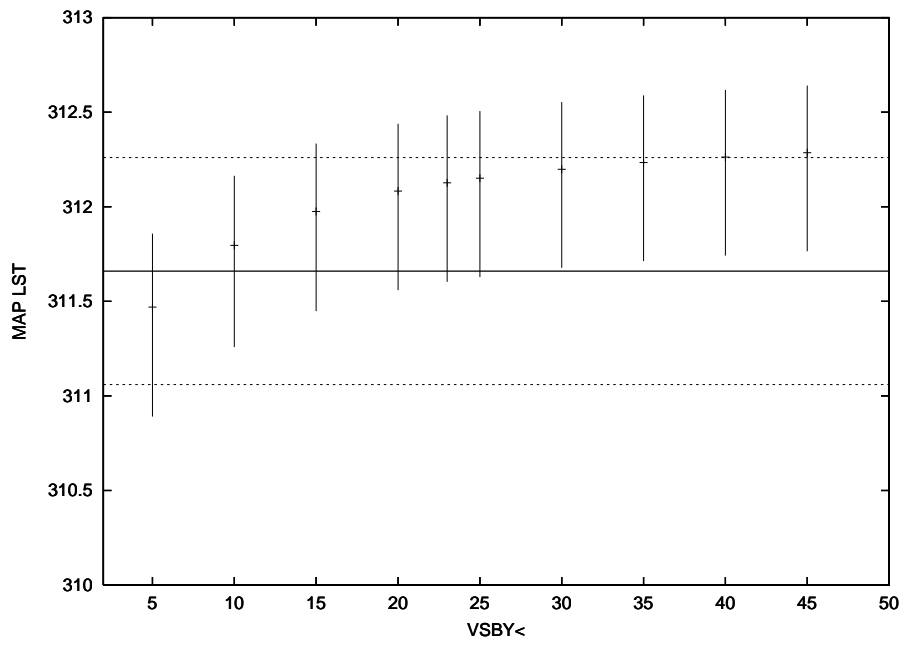


Figure .9: MAP LST estimates, confidence intervals marginalized on emissivity and  $VSBY_{<}$  vs.  $VSBY_{<}$  for DOY 2006/350. The horizontal lines show the MODIS LST value  $311.66 \pm 0.6K$  for this pixel.